J Neurophysiol 109: 1378–1390, 2013.
First published December 12, 2012; doi:10.1152/jn.00435.2012.

Slowly inactivating component of Na^+ current in peri-somatic region of hippocampal CA1 pyramidal neurons

Yul Young Park,[1,2] Daniel Johnston,[1] and Richard Gray[1]

[1]*Center for Learning and Memory, The University of Texas at Austin, Austin, Texas; and* [2]*Department of Biomedical Engineering, The University of Texas at Austin, Austin, Texas*

Submitted 23 May 2012; accepted in final form 7 December 2012

Park YY, Johnston D, Gray R. Slowly inactivating component of Na^+ current in peri-somatic region of hippocampal CA1 pyramidal neurons. *J Neurophysiol* 109: 1378–1390, 2013. First published December 12, 2012; doi:10.1152/jn.00435.2012.—The properties of voltage-gated ion channels on the neuronal membrane shape electrical activity such as generation and backpropagation of action potentials, initiation of dendritic spikes, and integration of synaptic inputs. Subthreshold currents mediated by sodium channels are of interest because of their activation near rest, slow inactivation kinetics, and consequent effects on excitability. Modulation of these currents can also perturb physiological responses of a neuron that might underlie pathological states such as epilepsy. Using nucleated patches from the peri-somatic region of hippocampal CA1 neurons, we recorded a slowly inactivating component of the macroscopic Na^+ current (which we have called I_{NaS}) that shared many biophysical properties with the persistent Na^+ current, I_{NaP}, but showed distinctively faster inactivating kinetics. Ramp voltage commands with a velocity of 400 mV/s were found to elicit this component of Na^+ current reliably. I_{NaS} also showed a more hyperpolarized *I-V* relationship and slower inactivation than those of the fast transient Na^+ current (I_{NaT}) recorded in the same patches. The peak amplitude of I_{NaS} was proportional to the peak amplitude of I_{NaT} but was much smaller in amplitude. Hexanol, riluzole, and ranolazine, known Na^+ channel blockers, were tested to compare their effects on both I_{NaS} and I_{NaT}. The peak conductance of I_{NaS} was preferentially blocked by hexanol and riluzole, but the shift of half-inactivation voltage ($V_{1/2}$) was only observed in the presence of riluzole. Current-clamp measurements with hexanol suggested that I_{NaS} was involved in generation of an action potential and in upregulation of neuronal excitability.

transient sodium current; persistent sodium current; subthreshold sodium current; hippocampus; sodium channel; neuronal excitability; hexanol; riluzole; ranolazine

THE VOLTAGE-GATED SODIUM CURRENT initiates and relays the neuronal action potential. The currents mediated by voltage-gated Na^+ channels in the brain are known to comprise at least three functionally distinctive Na^+ currents: transient, resurgent, and persistent. The transient Na^+ current (I_{NaT}) is activated rapidly and inactivates within a few milliseconds, contributing the majority of Na^+ influx during the upstroke of an action potential (Engel and Jonas 2005; Martina and Jonas 1997). A resurgent Na^+ current (I_{NaR}) is generated by rapid recovery of inactivated channels through open states, providing further depolarization immediately after repolarization, and facilitates high-frequency firing of the neuron (Raman and Bean 1997). The persistent Na^+ current (I_{NaP}) is a subthreshold regenerative conductance with a more negative activation voltage than I_{NaT} and has slowly inactivating or noninactivating characteristics (Crill 1996). I_{NaP} is generally believed to play prominent roles in action potential initiation, rhythmic firing, synaptic integration, subthreshold oscillation, and afterhyperpolarizations (Bean 2007; Crill 1996). A subthreshold component of Na^+ current in Purkinje and CA1 neurons that can be activated by excitatory postsynaptic potentials (EPSPs) has been recently described (Carter et al. 2012).

There have been several lines of evidence that there is a separate component of Na^+ current that activates at a subthreshold voltage range but inactivates on an intermediate timescale compared with those of transient and persistent Na^+ currents. The existence of a slowly inactivating, subthreshold Na^+ current has been suggested by previous observations of a second, slower component in Na^+ tail currents or inactivation kinetics (Benoit et al. 1985; Chiu 1977; Cummins et al. 1994; Gilly and Armstrong 1984; Huguenard et al. 1988). The presence of a subthreshold Na^+ conductance with intermediate inactivation kinetics has been identified in neurons from the suprachiasmatic nucleus (SCN) (Jackson et al. 2004; Kononenko et al. 2004), and in those cells a ramplike depolarization preceded action potential generation of the SCN neurons, which under voltage clamp corresponded to a slowly inactivating component (Pennartz et al. 1997).

It is difficult to study the different components of Na^+ current in isolation for multiple reasons. First, there is no specific pharmacological blocker to definitively isolate the separate components; all are sensitive to tetrodotoxin (TTX). Second, it is impossible to obtain an adequate space clamp (all membrane controlled at a set potential) of a pyramidal neuron with a complex topology (Spruston et al. 1993; Williams and Mitchell 2008). We chose to utilize the nucleated-patch technique (Martina and Jonas 1997) to achieve good space clamp and make quantitative measurements of the Na^+ current. Both step voltage commands and voltage ramps with varying velocities were used to separate the different components on the basis of their gating kinetics. We utilized ramp voltage commands to unveil the slower components of the Na^+ current that might play a role near threshold. The pharmacological agents hexanol, riluzole, and ranolazine were utilized to further separate the different components. In experiments designed to measure the roles of the different components of the Na^+ current, we used current-clamp recording to measure action potential generation, frequency of firing, and response to simulated synaptic inputs.

Address for reprint requests and other correspondence: R. Gray, Center for Learning and Memory, Univ. of Texas at Austin, 1, University Station Stop, C7000, Austin, TX 78712-0805 (e-mail: rick@mail.clm.utexas.edu).

MATERIALS AND METHODS

Slice preparation and recording conditions. Transverse hippocampal slices were prepared from 4- to 8-wk-old male Sprague-Dawley rats according to a protocol approved by the University of Texas at Austin Institutional Animal Care and Use Committee (IACUC) using methods previously described (Magee and Johnston 1995). All recordings were performed in the recording chamber, which was continuously perfused with artificial cerebrospinal fluid (ACSF). Borosilicate glass of 2.0-mm OD and 1.16-mm ID (Sutter Instrument, Novato, CA) was used to pull 4- to 6-MΩ patch electrodes with a Flaming/Brown P-97 micropipette puller (Sutter Instrument). All recordings were carried out near physiological temperature (31–34°C), and electrodes were wrapped in Parafilm to within ~200 μm from the tip to reduce electrode capacitance. For some experiments, 0.2% Neurobiotin was included in the recording pipette and the slices were fixed after recording with 3% glutaraldehyde. The fixed slices were processed with an avidin-HRP system activated by diaminobenzidine (DAB, Vector Labs) and then visualized with an AxioImager Z1 upright microscope (Carl Zeiss, Thornwood, NY).

Whole cell voltage-clamp recordings. Somatic whole cell voltage-clamp recordings were performed in CA1 pyramidal neurons. Bath saline contained (in mM) 125 NaCl, 3 KCl, 25 $NaHCO_3$, 2 $NiCl_2$, 1 $MgCl_2$, 10 dextrose, 1.3 ascorbic acid, and 3 Na^+ pyruvate, aerated with 95% O_2-5% CO_2. Pipette solution included (in mM) 10 CsCl, 120 Cs-gluconate, 10 HEPES, 4 NaCl, 0.1 3,4-diaminopyridine, 4 Mg-ATP, 0.3 Na-GTP, and 7 K_2-phosphocreatine, with pH 7.3 adjusted with TEA-OH. A slow ramp voltage protocol of 10 mV/s velocity was applied to inactivate all the transient Na^+ currents, leaving persistent inward Na^+ current. I_{NaP} was isolated either by subtracting traces recorded in the presence of TTX (TTX subtraction) or by subtracting a fitted line to a point more negative than −60 mV from the whole trace (linear leak subtraction). For some cases, the apical dendrite of the neuron was cut by a motorized blade under the microscope (Kang and Schuman 1996). The ramp current signals were amplified with an Axopatch 200B (Axon Instruments; Molecular Devices, Sunnyvale, CA), sampled at 10 or 50 kHz, and filtered off-line at 0.5 or 1 kHz. The measured liquid junction potential of −7.5 mV was not corrected. Input resistance (R_N) was monitored by a 10-mV hyperpolarized pulse in 30 ms from a holding potential (V_{hold}) of −65 mV. Cell capacitance was calculated by integrating a transient capacitive current evoked by the same pulse. Series resistance was estimated by dividing the time constant of the single-exponential fit to the transient capacitive current by the calculated cell capacitance. Series resistance (23.0 ± 2.5 MΩ; $n = 30$) was compensated by the built-in circuit of the amplifier (up to 85% prediction and 70% correction).

Nucleated-patch voltage-clamp recordings. Nucleated-patch recordings were made by slowly withdrawing the electrode while applying negative pressure after forming a whole cell recording (Martina and Jonas 1997). Bath saline and pipette solutions were the same as those in whole cell voltage-clamp experiments. Nucleated patches had R_N around 3 GΩ (2.92 ± 0.13 GΩ; $n = 69$), and patch capacitance was calculated from the patch size in the image captured from a Newvicon tube camera (Dage-MTI, Michigan City, IN), assuming 1 μF/cm^2. Series resistance (8.1 ± 0.5 MΩ; $n = 12$) was compensated up to 85% prediction and 60% correction, and maximum voltage error was <3 mV.

Currents in response to ramp voltage commands were corrected for leakage current by subtracting traces recorded in the presence of TTX (TTX subtraction) or by subtracting a line fit to points more negative than −60 mV from the whole trace (linear leak subtraction). Currents in response to step commands were corrected for leakage and capacitive currents by subtracting the scaled leak traces generated by 1/10 or 1/5 amplitude of voltage commands from the raw traces (P/−N protocol, N = 5 or 10). For the activation conductance-voltage (G-V) curves, a series of depolarizing step voltage commands from −70 to +10 mV in steps of 10 mV for 30 ms with $V_{hold} = -80$ mV were applied with a 2- to 3-s interval (activation protocol). The conductance (G_{Na}) was calculated by Ohm's law, $G_{Na} = I_{Na}/(V_{cmd} - E_{Na})$ where V_{cmd} is the command voltage and E_{Na} is the Na^+ reversal potential (+93.87 mV calculated from $[Na^+]_{in}$ and $[Na^+]_{out}$). The normalized conductance was plotted against voltage command. For the steady-state inactivation curve, 500-ms prepulses to voltages varying from −90 mV to −10 mV in steps of 10 mV were followed by a constant 30-ms test pulse to 0 mV with $V_{hold} = -90$ mV (inactivation protocol). Peak amplitude of current during a test voltage command was normalized and plotted versus prepulse potential. The voltage command protocol for the onset of I_{NaT} inactivation consists of V_{hold} of −80 mV, a prepulse (ranged from −60 to −10 mV by 10 mV) to test membrane potential (V_{test}) with various time intervals (Δt; 1–1,000 ms), and a following test voltage step to 0 mV in 30 ms. The peak amplitudes of I_{Na} traces elicited by V_{test} with increasing durations were normalized by that of I_{Na} with $\Delta t = 0$. The fraction of the Na^+ channels available was then plotted against Δt. The kinetics of recovery of I_{NaT} inactivation was measured by the standard double-pulse protocol consisting of V_{hold} of −80 mV, a conditioning pulse to −0 mV in 500 ms, a pulse to V_{rec} (ranged from −80 to −60 mV by 10 mV) with various time intervals (Δt; 1–1,000 ms), and a following test pulse to 0 mV in 30 ms. The peak amplitudes of I_{Na} traces elicited by the test pulse after holding at V_{rec} with increasing durations (Δt) were normalized by that of I_{Na} by the conditioning pulse. The fraction of the Na^+ channels recovered from the inactivation was then plotted against Δt. The I_{NaT} traces for the kinetics of deactivation were elicited by voltage protocols: −80 mV hyperpolarizing in 50 ms followed by 300-μs depolarization at 0 mV and repolarization at various potentials from −40 mV to −100 mV by 10 mV in 30 ms. The ramp current signals were processed in the same manner as in whole cell voltage-clamp experiments. The step current signals amplified by the Axopatch 200B were filtered at 5–20 kHz and sampled at 50 or 200 kHz.

Whole cell current-clamp recordings. The ACSF contained (in mM) 125 NaCl, 3 KCl, 1.25 NaH_2PO_4, 25 $NaHCO_3$, 2 $CaCl_2$, 1 $MgCl_2$, 10 dextrose, 1.3 ascorbic acid, and 3 Na^+ pyruvate, aerated with 95% O_2-5% CO_2. The pipette solution contained (in mM) 20 KCl, 120 K-gluconate, 10 HEPES, 4 NaCl, 4 Mg-ATP, 0.3 Na-GTP, and 7 phosphocreatine, with pH adjusted to 7.3 with KOH. Voltage signals were amplified and filtered at 5 kHz with a BVC-700A amplifier (Dagan, Minneapolis, MN) and sampled at 40 kHz. Access resistance and resting membrane potential were monitored throughout the experiment online. Access resistance was compensated with the amplifier's bridge circuit and was ≤30 MΩ. Resting membrane potential was in the range of −68 to −60 mV.

Drug application. TTX (0.5 μM) and hexanol (1.4 mM) were bath applied for current-clamp experiments. For nucleated-patch recordings, 2 μM TTX, 2.8 mM hexanol, 10 μM riluzole, or 30 μM ranolazine was included in a puffer pipette that also contained (in mM) 149 NaCl, 3 KCl, 1 $MgCl_2$, 10 HEPES, 2 $NiCl_2$, 10 dextrose, 1.3 ascorbic acid, and 3 Na^+ pyruvate, with pH adjusted to 7.3 with NaOH. A pair of puffer pipettes of 3- to 4-μm diameter was pulled, and one electrode was loaded with Fast Green dye in order to confirm the diffusion pattern of puffing. The other electrode was loaded with the drug being used for that experiment, and the patch was located in the drug diffusion region identified by the dye. Drugs were applied by a pressurized injection system (Picospritzer II, General Valve, Fairfield, NJ) or passive release of pressure via a check valve. There was often a small effect on measured currents during puffer application of saline for control experiments (presumably due to mechanical effects). Therefore, all measurements were compared to the saline controls. When it was necessary for a neuron to be isolated from the network, all AMPA, NMDA, $GABA_A$, and $GABA_B$ receptor-mediated synaptic transmissions were blocked by CNQX (10 μM) or DNQX (20 μM), DL-AP-5 (50 μM), bicuculline (10 μM in DMSO) and picrotoxin (10 μM in ethanol), and (2S)-3-[[(1S)-1-(3,4-dichlorophenyl)ethyl]-

amino-2-hydroxypropyl] (phenylmethyl)phosphinic acid (CGP55845; 2 μM in DMSO), respectively. A riluzole stock at 1 mM was made by dissolving it into DMSO and diluted with puffing solution to the final concentration of 10 μM right before the experiment. The total amount of DMSO in external solution remained below 0.1%, and the total amount of ethanol in the bath was maintained below 0.05%. The chemicals for ACSF were purchased from Fisher Scientific (Pittsburgh, PA), TTX from Ascent Scientific (Princeton, NJ), riluzole and ranolazine from Tocris (Ellisville, MO), and the other chemicals from Sigma-Aldrich (St. Louis, MO).

Data collection and analysis. Data acquisition, stimulus generation, and analysis were performed with an Instrutech ITC-18 DA/AD converter (HEKA Instruments, Bellmore, NY) controlled by IGOR Pro (WaveMetrics, Portland, OR) software on an Apple computer (Cupertino, CA) using locally written procedures. Amplified signals were filtered up to 20 kHz by the low-pass filter built into the amplifier or an external low-pass filter (model 902, Frequency Devices, Ottawa, IL). All Na^+ current traces were averaged from three to seven individual traces. For nucleated-patch recordings, I_{NaS} and I_{NaT} were quantified with activation and inactivation curves that were fitted by a Boltzmann equation, $f(x) = \text{base} + \max/\{1 + \exp[-(x - V_{1/2})/k]\}$, resulting in half-activation and half-inactivation voltage ($V_{1/2}$) and k values for I_{NaS} and I_{NaT}. The activation kinetics of I_{NaT} was fitted by a cubic exponential function, $f(x) = A \times \{1 - \exp[-(x - x_0)/\tau_m]\}^3$, and the kinetics of inactivation and deactivation were obtained by fitting the corresponding graphs to a single-exponential $\{f(x) = f_0 + A \times \exp[-(x - x_0)/\tau]\}$ or double-exponential $\{f(x) = f_0 + A_1 \times \exp[-(x - x_0)/\tau_{fast}] + A_2 \times \exp[-(x - x_0)/\tau_{slow}]\}$ function, depending on the testing potentials (Engel and Jonas 2005; Martina and Jonas 1997). Exponential fits were made to the data with DISCRETE (Provencher 1976). For current-clamp recording, a frequency vs. current injection (F-I) curve was made by counting the number of spikes evoked by step current injections from 0 to 180 pA in 30-pA increments. Currents simulated by an α-function, $A(t/\alpha)e^{(-\alpha t)}$, where A is the amplitude of injected current, t is time, and $1/\alpha$ is the time to peak, were injected to mimic EPSPs (α-EPSP injection). With this shape of current injection, temporal summation (α-EPSP summation) of the neuron was quantified by counting the number of spikes generated by α-EPSP injections at 25 Hz. Statistical tests performed were Mann-Whitney test (for 2 groups, unpaired data), unpaired and paired t-test (for 2 groups, unpaired and paired data), Kruskal-Wallis test and post hoc Dunn's test (for >3 groups, unpaired data), and linear regression/correlation test. Markers and error bars in Figs. 1 and 3–8 indicate means ± SE.

RESULTS

Our initial interest was in the role of the persistent Na^+ current in intrinsic plasticity of CA1 pyramidal cells, so we first confirmed the existence of I_{NaP} in hippocampal CA1 pyramidal neurons (Fig. 1*A*, *top*). Using techniques similar to those of others (Fleidervish and Gutnick 1996; Magistretti and Alonso 1999; Wu et al. 2005), we used ramp voltage commands with four different velocities: 400, 100, 40, and 10 mV/s. The slowest ramp voltage command of 10 mV/s reliably inactivated transient Na^+ currents, leaving inward Na^+ current identified as I_{NaP} (Fig. 1*A*, *middle*), but faster ramp velocities evoked Na^+ currents contaminated by uncontrolled, escape Na^+ spikes (data not shown). The slow inactivation of I_{NaP} was obvious from the inward current during the downslope of triangular voltage commands (Fig. 1*A*, *bottom*). When the apical dendrites of CA1 pyramidal neurons were cut in an attempt to improve space-clamp conditions (Fig. 1*B*, *top*), the amplitude of I_{NaP} was smaller than that of the intact neuron (Fig. 1*B*, *middle* and *bottom*), suggesting the presence of I_{NaP} in dendrites. Compared with the intact neurons, the dendrotomized neurons showed a significant increase in R_N (147.7 ± 8.6 vs. 429.6 ± 62.9 MΩ; $P < 0.0001$, Mann-Whitney test; Fig. 1*C*) and a decrease in cell capacitance (254.0 ± 10.0 vs. 152.8 ± 17.7 pF; $P < 0.0001$, Mann-Whitney test; Fig. 1*D*) and I_{NaP} amplitude (−477.6 ± 26.0 vs. −91.0 ± 12.4 pA; $P < 0.0001$, Mann-Whitney test; Fig. 1*E*), suggesting resealing of the cut ends.

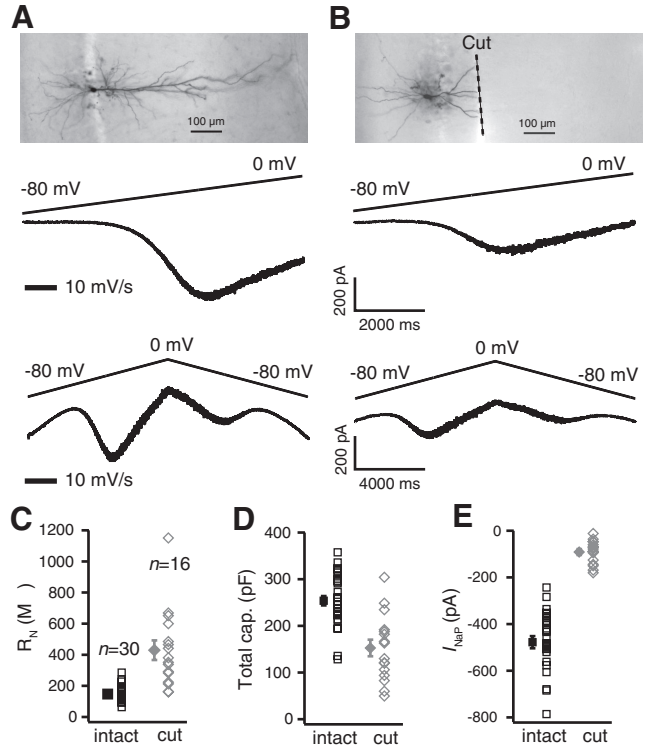

Fig. 1. Persistent Na^+ currents in intact and dendrotomized CA1 pyramidal neurons. *A*: a hippocampal CA1 pyramidal neuron (*top*) showed persistent Na^+ current that was evoked by a slow (10 mV/s) ramp voltage command (*middle*) and partially inactivated in seconds in response to a triangle command (*bottom*). *B*: a neuron with its dendrite cut (*top*) showed reduced peak amplitude of persistent Na^+ current (*middle*) and similar slow inactivation (*bottom*). *C–E*: summary of differences in input resistance (R_N, *C*), cell capacitance (*D*), and peak amplitude of persistent Na^+ current (I_{NaP}, *E*) between intact and dendrotomized neurons.

Because of the well-known lack of space clamp in pyramidal neurons from somatic whole cell voltage clamping and the possible effects of poor clamp on activation/inactivation kinetics, we decided to utilize nucleated patches for our analysis (see MATERIALS AND METHODS) (Fig. 2*A*) (Martina and Jonas 1997). Surprisingly, a 10 mV/s velocity ramp voltage command was unable to elicit detectable I_{NaP} in the nucleated-patch recordings (Fig. 2*B1*). Faster ramp voltage commands of 40 or 100 mV/s ramp elicited only a very small inward current, but a 400 mV/s ramp command evoked an inward Na^+ current that could be measured reliably. Figure 2*B1* shows an example trace of the inward Na^+ ramp current with peak amplitude of 7.0 pA (6.5 ± 0.8 pA, $n = 3$), where the peak transient Na^+ current amplitude evoked by a voltage step from −80 to 0 mV was 237 pA (216 ± 11 pA, $n = 3$). This inward Na^+ ramp current showed faster inactivation than that of I_{NaP} in response to a triangular voltage command (Fig. 2*B2*, *bottom*; $n = 7$) and could be blocked by puffer application of 2 μM TTX (Fig. 2*B2*, *top*).

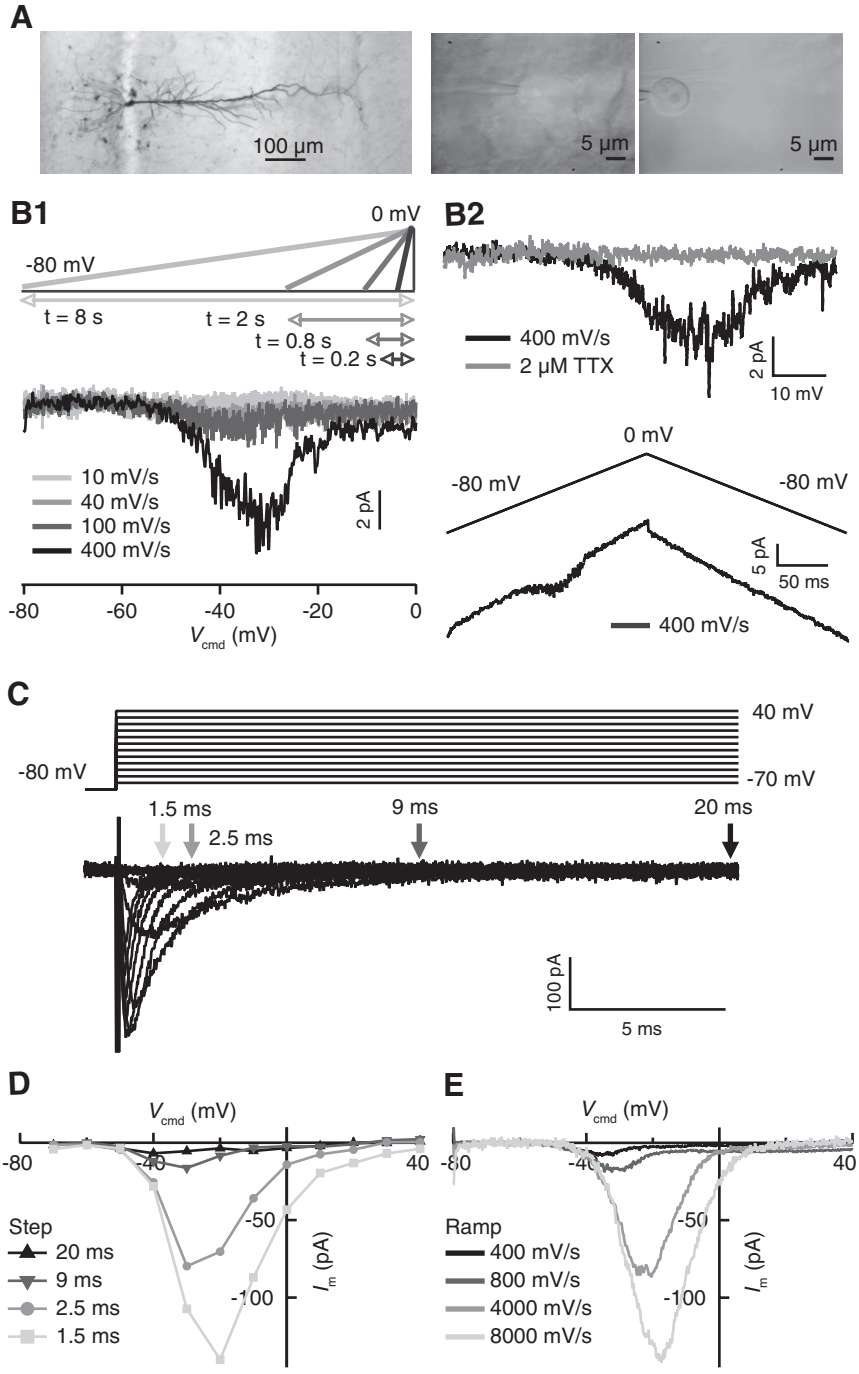

Fig. 2. Slowly inactivating, subthreshold Na^+ current in hippocampal CA1 pyramidal neurons. *A*: example images of an intact CA1 pyramidal neuron (*left*), during whole-cell recording (*center*), and subsequent nucleated-patch configuration (*right*). *B1*: current traces in response to ramp commands (V_{cmd}) with different velocities from nucleated patches. Ramps with velocity of 400 mV/s generated a small but reliable inward current (7 pA), while the slower ramp commands elicited currents too small to measure. *B2*: inward current was blocked by 2 μM TTX by puffer application (*top*). During the falling phase of a triangle clamp the inward current was totally inactivated (*bottom*). *C*: Na^+ currents evoked by step voltage commands from −70 to 40 mV with a holding potential (V_{hold}) of −80 mV. Amplitudes of Na^+ currents from step commands were measured at 1.5, 2.5, 9, and 20 ms. *D*: currents (I_m) measured at 4 time points are plotted against voltage command. *E*: currents evoked by 4 different ramp velocities are plotted against voltage command.

Despite this lack of persistence, the ramp current showed a voltage-dependent activation similar to that of I_{NaP}. We empirically compared current-voltage (*I-V*) curves from step and ramp voltage commands to determine whether the slowly inactivating inward Na^+ currents elicited by 400 mV/s ramps corresponded to the late Na^+ currents from step commands. I_{Na} (leak-corrected by linear subtraction) was measured at four different time points after the onset of the step voltage command (Fig. 2*C*). *I-V* curves were then constructed at each time point by measuring the current amplitude during the command (Fig. 2*D*). As time increased, there was a decrease in peak amplitude and a leftward shift of the peak of the *I-V* curves revealing an inward current with small amplitude at later time points. Ramp command voltages of much faster velocities (400, 800, 4,000 and 8,000 mV/s; Fig. 2*E*) were applied to determine which produced the best separation of the fast, transient current from the slowly inactivating inward Na^+ current. As the ramp velocity decreased, the peak current amplitude also decreased and the peak current shifted to more negative potentials ($n = 4$). The ramp current with a velocity of 400 mV/s most closely matched the late (20 ms) current recorded from step commands. Therefore, this slowly inactivating component of Na^+ current evoked by 400 mV/s ramp voltage command was measured in subsequent experiments. Our working hypothesis is that the fastest ramp velocity (4,000–8,000 mV/s) elicits the fast I_{NaT} and slower velocities

unveil the slower components of Na^+ current, with its peak occurring with a ramp velocity of ~400 mV/s. We called the slow component evoked by the 400 mV/s ramp voltage command "I_{NaS}," a previous notation for the Na^+ current with similar properties in SCN neurons (Kononenko et al. 2004).

Na^+ currents in nucleated-patch recordings. We performed nucleated-patch experiments to measure I_{NaT} and compare this to the components of Na^+ current with slower inactivation kinetics (I_{NaS}). The voltage-dependent activation of I_{NaT} was determined by an activation protocol (see MATERIALS AND METHODS), and the resulting activation *G-V* curve showed half-activation voltage $V_{1/2} = -21.0 \pm 0.7$ mV and slope factor $k = 6.3 \pm 0.1$ (Fig. 3, *A* and *C*). The voltage dependence of inactivation for I_{NaT} was determined by an inactivation protocol, and the availability curve showed $V_{1/2} = -56.3 \pm 1.2$ mV and $k = 5.4 \pm 0.1$ (Fig. 3, *B* and *C*). We also characterized the activation kinetics (τ_{act}) of I_{NaT} over the range of −30 to +40 mV (Fig. 3*D*). The rapid rise of I_{NaT} activation was fit with a cubic exponential function with a small delay. As the test voltage increased, τ_{act} became smaller. With a wideband low-pass filter (20 kHz) and high sampling frequency (200 kHz), we were able to measure τ_{act} (22.2 ± 2.3 μs at 40 mV) (Fig. 3*F*, *top*). The time course of I_{NaT} deactivation was also investigated (Fig. 3*E*). The deactivation time constant (τ_{deact}) was obtained by fitting the trace with a single-exponential function at most test potentials, reaching 38.0 ± 3.5 μs at −100 mV (Fig. 3*F*, *bottom*), but the trace evoked by the −40 mV test potential was best fit by a double exponential.

The time constant of inactivation (τ_{inact}) was measured from the decay of the current evoked by test voltage command of 100-ms duration at potentials from −30 to +40 mV. The current traces were leak subtracted with TTX (at 50-kHz sampling and 5-kHz low-pass filtering), and were best fit with a double exponential, generating a negligible residual compared with a single-exponential fit (Fig. 4*A*). Both $\tau_{inact,fast}$ and $\tau_{inact,slow}$ decreased with increasing test voltage (Fig. 4*B*, *top*), and the relative amplitudes of the fast ($\tau_{inact,fast}$) and slow ($\tau_{inact,slow}$) components are shown in Fig. 4*B*, *bottom*. The increase in the duration of inactivation prepulse shifted the availability curve to more hyperpolarized potentials (Fig. 4*C*). We measured the kinetics of the onset of inactivation with a prepulse protocol with increasing duration to further examine the inactivation occurring at subthreshold voltage ranges (Fig. 4*D*). The peak Na^+ currents evoked after prepulses of various durations (Δt) at V_{test} were normalized to the Na^+ current evoked without a prepulse and plotted against prepulse duration. The normalized Na^+ peak amplitude was fit by a double-exponential function. The relative contributions of fast and slow components (in %) were 53.7:46.3 (−60 mV), 50.9:49.1 (−50 mV), 29.9:70.1 (−40 mV), 37.6:62.4 (−30 mV), 48.6:51.4 (−20 mV), and 54.7:45.3 (−10 mV) at respective test voltages. The time course of development of inactivation

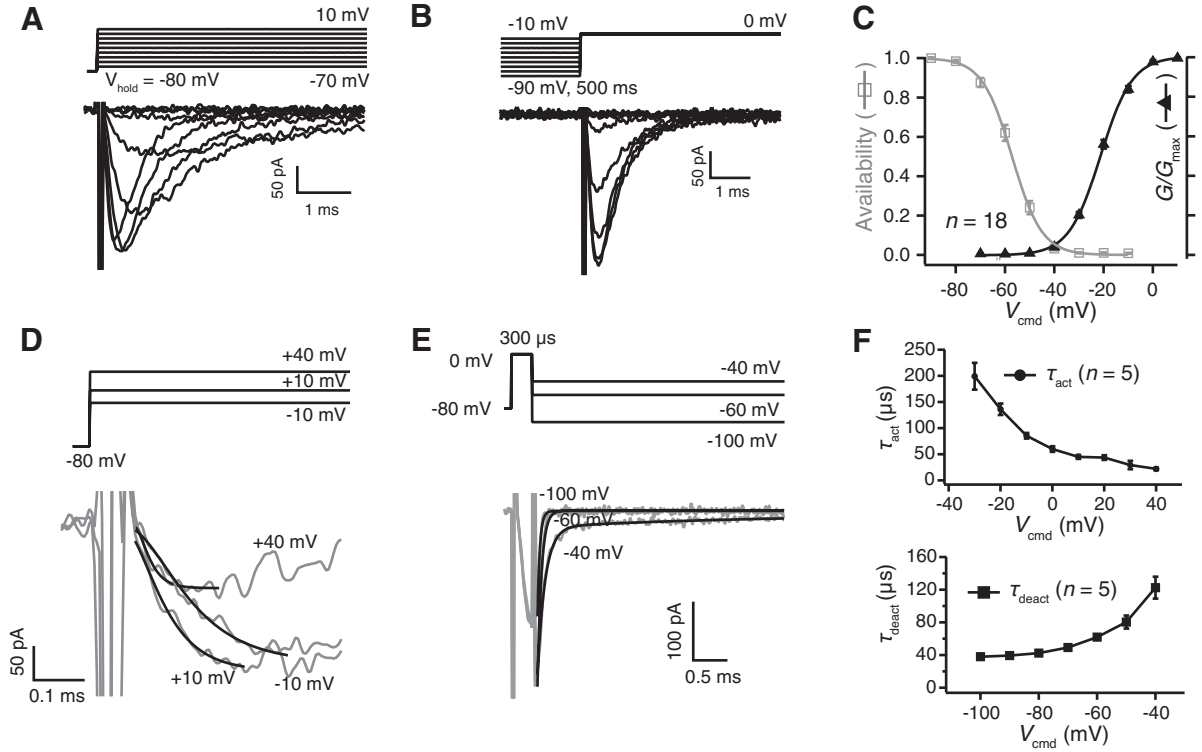

Fig. 3. Characterization of transient Na^+ current (I_{NaT}) in nucleated patch recordings. *A* and *B*: example traces of I_{NaT} generated by the activation (*A*) and inactivation (*B*) protocols (see MATERIALS AND METHODS). *C*: normalized steady-state inactivation (gray) and activation (black) conductance (G/G_{max}) curves of I_{NaT}. Curves were fit to a single Boltzmann function. The inactivation curve gave −56.3 ± 1.2 mV for $V_{1/2}$ and 5.4 ± 0.1 for slope factor *k*. G/G_{max} gave $V_{1/2} = -21.0 \pm 0.7$ mV and $k = 6.3 \pm 0.1$. *D*: kinetics of onset of I_{NaT} activation. Currents were fit by a cubic exponential function to determine the activation time constant, τ_{act} (see MATERIALS AND METHODS) Black lines overlie the raw curves (gray). Time constants (τ_{act}) were 84.0, 55.9, and 23.1 μs at −10, +10, and +40 mV, respectively. *E*: time course of I_{NaT} deactivation (τ_{deact}) was measured by fitting I_{NaT} tail currents with a single- or double-exponential function. The I_{NaT} tail current evoked by −40 mV test pulse showed a biexponential time course ($\tau_{deact,fast} = 112$ μs and $\tau_{deact,slow} = 2.99$ ms), while more negative test commands showed a single-exponential time course ($\tau_{deact} = 57.6$ μs at −60 mV and 35.1 μs at −100 mV test pulse). *F*: summary plots: τ_{act} from −30 to + 40 mV (*top*) and τ_{deact} at voltages from −40 to −100 mV (*bottom*). All traces were corrected by P/−N leak subtraction.

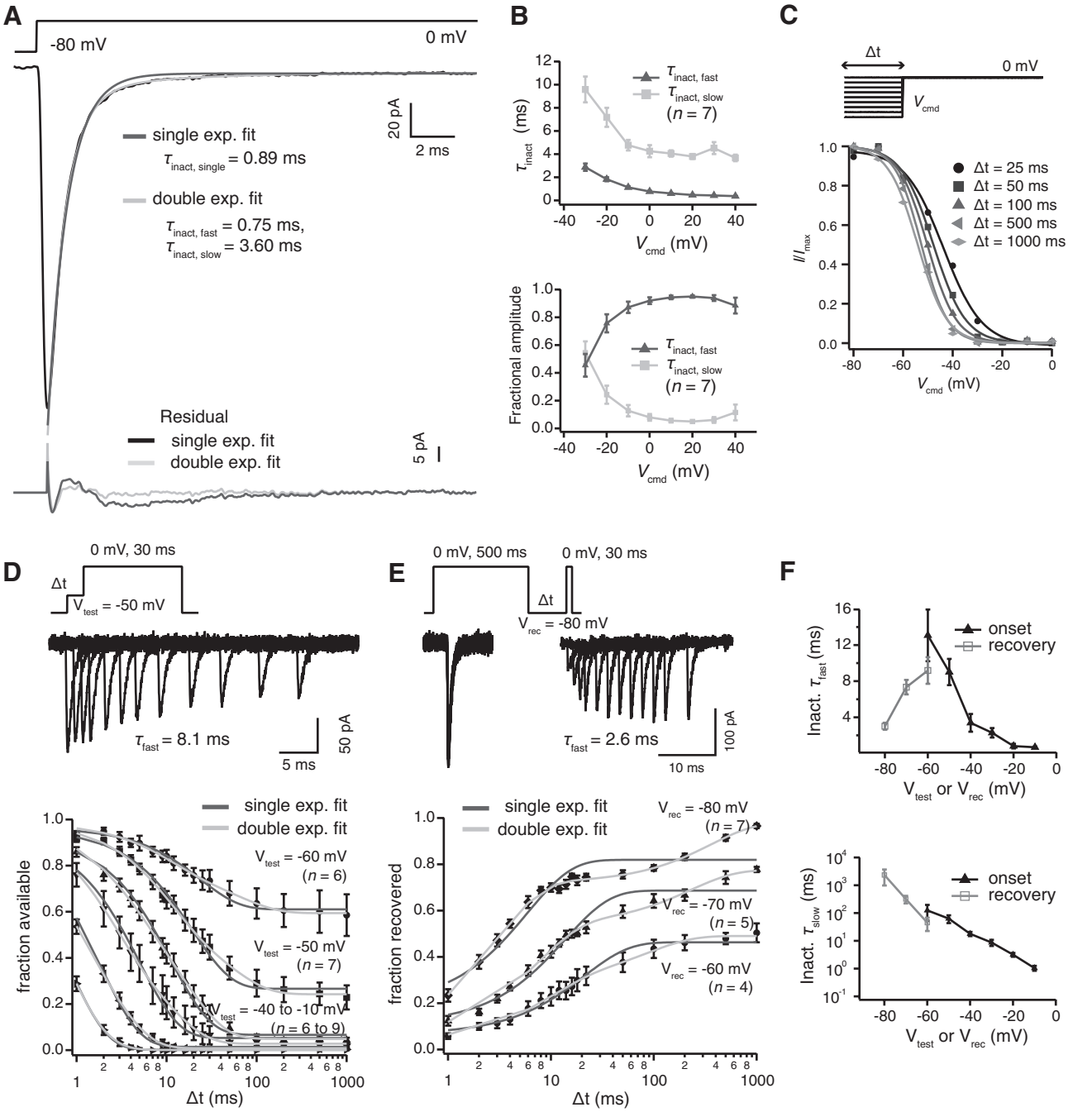

Fig. 4. Inactivation of I_{NaT} in nucleated patch recordings. *A*: time course of I_{NaT} inactivation was measured by fitting the decay phase of I_{NaT} with a double-exponential function. A double exponential provided a better fit than a single exponential illustrated by the plots of residuals (*bottom*). *B*: summary plots: τ_{inact} from −30 to + 40 mV (*top*) and fractional amplitude of fast and slow components in inactivation (*bottom*). *C*: prepulses from −80 to 0 mV with increasing duration (*top*) caused the left shift ($\Delta V_{1/2}$ = −10.4 mV) of $V_{1/2}$ and a steeper (Δk = −1.8) slope factor of steady-state inactivation curve (*bottom*) from the same patch. *D*: onset of inactivation was measured with a double-pulse protocol with prepulses of increasing duration at voltages (V_{test}) from −60 to −10 mV. Na^+ current traces at V_{test} = −50 mV are shown, and the normalized peak Na^+ current amplitude (*bottom*) at V_{test} = −60 to −10 mV was fit with a double-exponential function. *E*: time course of recovery from inactivation was measured by double-pulse protocols. Na^+ current traces (*top*) at V_{rec} = −80 mV are shown, and the normalized peak Na^+ current amplitudes (*bottom*) at V_{rec} = −80 to −60 mV were fit with a double-exponential function. *F*: resulting summary plot of time constants of onset and recovery from inactivation: τ_{fast} (*top*) and τ_{slow} (*bottom*). All traces were corrected by P/−N leak subtraction except in *A* and *B*, which were corrected with TTX leak subtraction.

measured by the prepulse protocol was similar to the decaying kinetics of the Na^+ currents at −30 mV (P = 0.447 for $\tau_{inact,fast}$ and 0.828 for $\tau_{inact,slow}$; unpaired t-test) but significantly faster at −20 and −10 mV ($P < 0.05$). The kinetics of recovery from inactivation was studied with a double-pulse protocol (Fig. 4*E*). It consisted of a 500-ms prepulse to 0 mV and a second pulse to 0 mV for 30 ms with variable time intervals (Δt) at several membrane potentials for the recovery (V_{rec}). The peak Na^+ currents evoked by the second pulse were normalized by the peak Na^+ current of the first pulse and

plotted against Δt. The normalized Na^+ peak amplitude showed a double-exponential component at recovery voltages between −60 and −80 mV. The relative contributions of fast and slow components (in %) were 50.2:49.8 at −60 mV, 63.5:36.5 at −70 mV, and 73.9:26.1 at −80 mV, respectively.

Using the fast and slow inactivation time constants obtained above (Fig. 4), we reconstructed a step *I-V* curve at different time points for different test potentials for the same data set in Fig. 2, *C–E* ($n = 4$). Assuming $\tau_{inact,slow} = 4 \times \tau_{inact,fast}$, we chose $t = 3 \times \tau_{inact,fast}$ where the fast component was inactivated by ~95% and the slow component inactivated ~50%. The resulting Fig. 5*A* allowed us to visualize how the voltage ramp protocol, where both time and voltage are changing, can cause significant voltage inactivation at higher depolarization potentials. However, the initial phase of increasing ramp current at hyperpolarized potentials was closely matched to the step *I-V* at corresponding voltages, and it enabled us to use the ramp protocol as an effective method to assess "I_{NaS}."

When we recorded both I_{NaS} and I_{NaT} ($n = 18$) from the same patches, we found that G_{NaS} calculated in the same manner as G_{NaT} showed a more negative $V_{1/2}$ (−37.7 vs. −21.0 mV) and smaller k (3.7 vs. 6.3) than G_{NaT} (Fig. 5*B*). We examined the relationship between I_{NaS} and I_{NaT} recorded from the same nucleated patches ($n = 110$). The peak amplitude of I_{NaS} occurred around −40 to −30 mV with a 400 mV/s ramp command and averaged −5.16 ± 0.22 pA, while that of I_{NaT}, measured from step commands, peaked at −10 to +10 mV with an amplitude of −174.6 ± 7.8 pA. The relationship of peak amplitudes of I_{NaT} to I_{NaS} was linear and the ratio I_{NaS}/I_{NaT} was 0.0238 (Pearson's correlation test, $r = 0.839$; $P < 0.0001$; $n = 110$), indicating that the amplitude of I_{NaS} is ~2.38% of I_{NaT} from nucleated patches (Fig. 5*C*).

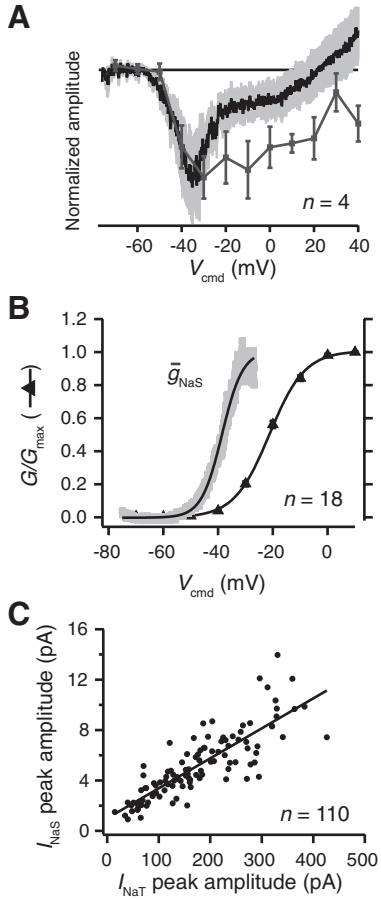

Fig. 5. *A*: amplitude of Na^+ currents evoked by step protocol was measured at $t = 3 \times \tau_{inact,fast}$ after activation of the current and overlaid onto the average current generated by 400 mV/s ramp protocol (the same data set as in Fig. 2, *C–E*). *B*: comparison of voltage dependence of I_{NaS} and I_{NaT} activation. Normalized conductance of I_{NaS} ($G/G_{max,NaS}$) was plotted with the activation *G-V* curve from recordings of I_{NaT} (copied from Fig. 3*C*) from the same patch. The activation *G-V* curve of I_{NaS} gave $V_{1/2} = -37.7 \pm 1.0$ mV and $k = 3.7 \pm 0.2$ compared with $V_{1/2} = -21.0 \pm 0.7$ mV and $k = 6.3 \pm 0.1$ for I_{NaT}. *C*: relationship between the peak amplitudes of I_{NaS} and I_{NaT}: both I_{NaS} and I_{NaT} recorded from the same patch showed a linear correlation (Pearson's $r = 0.839$). The peak amplitude of I_{NaS} was 2.38% of the peak I_{NaT}.

Effects of pharmacological blockers on I_{NaS} and I_{NaT}. We tested several known Na^+ channel blockers for their ability to block I_{NaS}. We have shown in earlier experiments that TTX fully blocks all I_{Na}. Hexanol, one of the *n*-alcohols known to block I_{NaT} (Horishita and Harris 2008; Shiraishi and Harris 2004) and to have anesthetic effects (Alifimoff et al. 1989), was chosen because of its strong potency with relatively low concentration compared with other alcohols with a shorter carbon chain such as ethanol and butanol. Hexanol at 2.8 mM (a moderate anesthetic concentration) suppressed both I_{NaS} and I_{NaT}, but to different degrees. Puff application of hexanol on the nucleated patch reduced the amplitude of I_{NaS} by 64.7% (Fig. 6*A*) and of I_{NaT} by 31.1% (Fig. 6*B*). The maximum conductance of I_{NaS} elicited by a 400 mV/s ramp voltage command was reduced significantly in the presence of hexanol (Fig. 6*C*).

We further investigated this differential block of I_{NaS} and I_{NaT} with two additional drugs, riluzole (10 μM) and ranolazine (30 μM), both previously reported to block persistent Na^+ current (Benoit and Escande 1991; Rajamani et al. 2009). None of the three drugs caused a significant change in $V_{1/2}$ of activation (Fig. 6*D*). However, hexanol and riluzole, but not ranolazine, caused a significant reduction in $G_{NaS,max}$ (drug − saline = −49.7 ± 3.3% and −52.6 ± 3.4%, respectively; $P < 0.001$; Kruskal-Wallis test and post hoc Dunn's test). The results from the pharmacological experiments are summarized in Table 1.

We tested the effects of hexanol, riluzole, ranolazine, and saline on the activation *G-V* curve of I_{NaT}. Figure 6*E* illustrates the suppression of maximum conductance of I_{NaT} in the activation *G-V* curve by hexanol. No drugs revealed a significant change in voltage dependence of the channel activation (Fig. 6*F*). Hexanol and riluzole, but not ranolazine, decreased the maximum conductance of I_{NaT} to a lesser degree than that of I_{NaS} (drug − saline = −24.9 ± 8.0% and −22.4 ± 6.4%, respectively; $P < 0.05$; Table 1).

The effects of the drugs on steady-state inactivation of I_{NaT} were then tested. Hexanol application caused a decrease in the maximum amplitude of I_{NaT} (drug − saline = −21.1 ± 3.7%; Fig. 6*G*). We then tested riluzole and ranolazine and found that riluzole also decreased the maximum amplitude of I_{NaT} (−24.9 ± 3.3%). Ranolazine, however, had no significant effect on Na^+ current (Table 1). Among the three drugs, riluzole was the only one that produced a statistically significant left shift of $V_{1/2}$ of the steady-state inactivation curve (−9.2 ± 1.4 mV; $n = 4$; $P < 0.05$; Fig. 6*H* and Table 1). There was no significant change in the slope factor for any of the drugs.

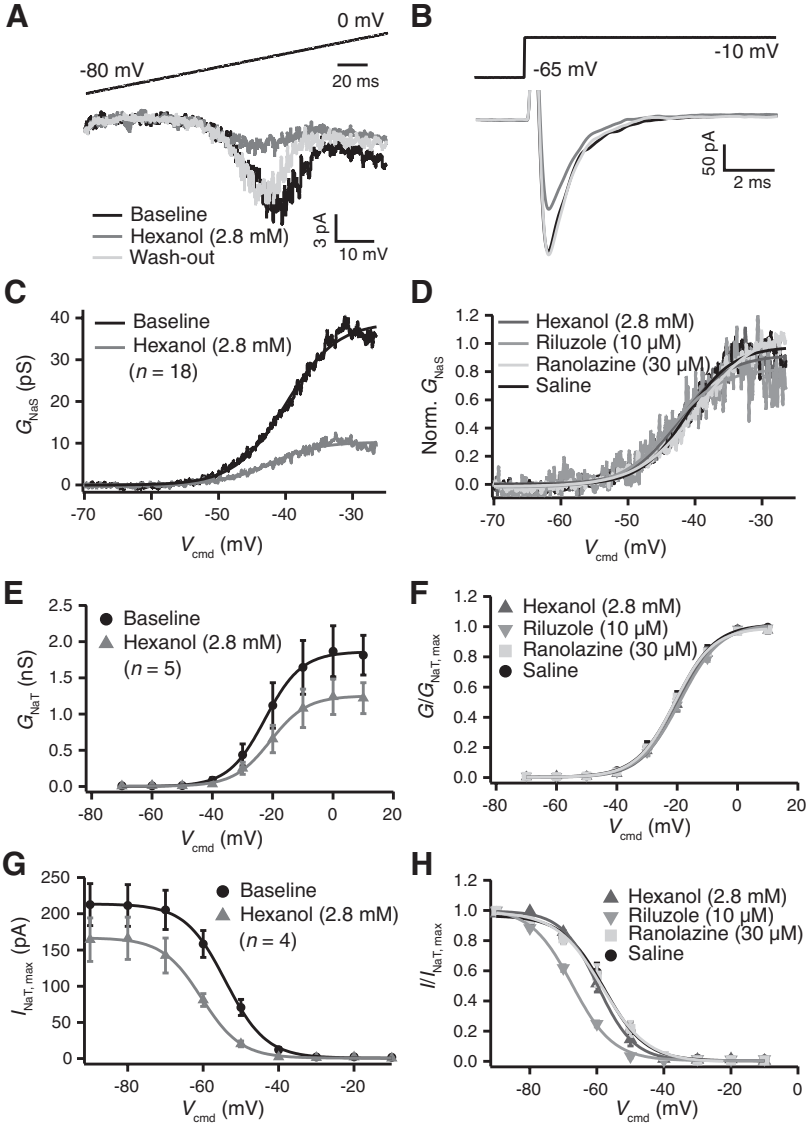

Fig. 6. Effects of Na^+ channel blockers on I_{NaS} and I_{NaT}. *A* and *B*: example traces of I_{NaS} and I_{NaT} showing reduction of current amplitude after hexanol application. I_{NaS} was reduced by 64.7% (*A*) and I_{NaT} by 31.1% (*B*). *C*: G_{NaS} showed a significant suppression by hexanol in a reversible manner. *D*: the early part of the *G-V* curve of I_{NaS} was fitted by a Boltzmann equation and the normalized *G-V* curves in 4 conditions (hexanol, riluzole, ranolazine, saline) were superimposed, indicating no change in voltage dependence of I_{NaS}. *E*: effect of hexanol on G_{NaT}. Hexanol caused a significant decrease in G_{NaT}. *F*: normalized activation *G-V* curve showed no significant change in voltage dependence under all tested conditions. *G*: effect of hexanol on the voltage dependence of inactivation of I_{NaT}. *H*: normalized steady-state inactivation curves showed a significant leftward shift of the curve only in the presence of riluzole.

In a different set of experiments, we tested the blocking of I_{NaT} in the presence of hexanol at a lower concentration (1.4 mM). We found that the lower concentration of hexanol caused a smaller blocking effect on peak I_{NaT} compared with 2.8 mM hexanol ($-18.4 \pm 2.3\%$; $P = 0.0002$, 1-sample *t*-test). We also tested the effect of hexanol on both fast and slowly inactivating components of Na^+ current in the nucleated patch (Fig. 7). In the presence of 2.8 mM hexanol, fast inactivation in the example traces shown in Fig. 7*A* was enhanced and the slowly inactivating component was blocked. Overall, the drug accelerated fast inactivation prominently at most test voltages and made the slow component less voltage sensitive (Fig. 7*B*, *bottom*). The reduction of fractional amplitude of the second component was statistically significant at -30 mV (Fig. 7*B*, *top*; $P = 0.018$).

I_{NaS} and neuronal excitability. We next investigated the physiological consequences of suppressing I_{NaS} with hexanol in current-clamp recordings from in situ hippocampal CA1

Table 1. *Effect of Na^+ channel blockers on I_{NaS} and I_{NaT}*

	I_{NaS}, Activation				I_{NaT}, Activation				I_{NaT}, Inactivation			
	n	$G_{NaS,\,max}$ change, %	$\Delta V_{1/2}$, mV	Δk	*n*	$G_{NaT,\,max}$ change, %	$\Delta V_{1/2}$, mV	Δk	*n*	$I_{NaT,\,max}$ change, %	$\Delta V_{1/2}$, mV	Δk
Hexanol	18	-71.1 ± 3.2‡	-3.01 ± 0.70	-0.45 ± 0.35	5	-35.3 ± 8.0*	2.05 ± 1.01	0.19 ± 0.14	4	-23.3 ± 4.1*	-6.10 ± 1.03	-0.16 ± 0.33
Riluzole	7	-73.9 ± 3.4‡	-4.48 ± 1.48	0.28 ± 0.83	5	-32.8 ± 6.4*	1.89 ± 0.73	0.41 ± 0.46	4	-27.1 ± 3.3†	-13.1 ± 1.41*	-0.90 ± 0.22
Ranolazine	12	-34.9 ± 5.0	0.55 ± 0.70	0.88 ± 0.22	7	-25.0 ± 1.5	1.84 ± 0.48	0.10 ± 0.25	7	-14.2 ± 1.6	-3.34 ± 0.47	-0.52 ± 0.20
Saline	11	-21.4 ± 4.6	-1.54 ± 0.60	-0.10 ± 0.30	5	-10.4 ± 2.3	-0.55 ± 0.65	0.07 ± 0.49	5	-2.20 ± 3.1	-3.84 ± 0.34	-0.62 ± 0.53

Values are means ± SE. The effect of each drug was compared with the saline condition. Maximum conductance G_{max} (or current amplitude I_{max}) change was calculated by $(G_{max,Drug} - G_{max,Baseline})/G_{max,Baseline} \times 100$; $\Delta V_{1/2}$ (or Δk) was calculated by $V_{1/2,\,Drug} - V_{1/2,\,Baseline}$ (or $k_{Drug} - k_{Baseline}$). Kruskal-Wallis test and post hoc Dunn's test: *$P < 0.05$; †$P < 0.01$; ‡$P < 0.001$.

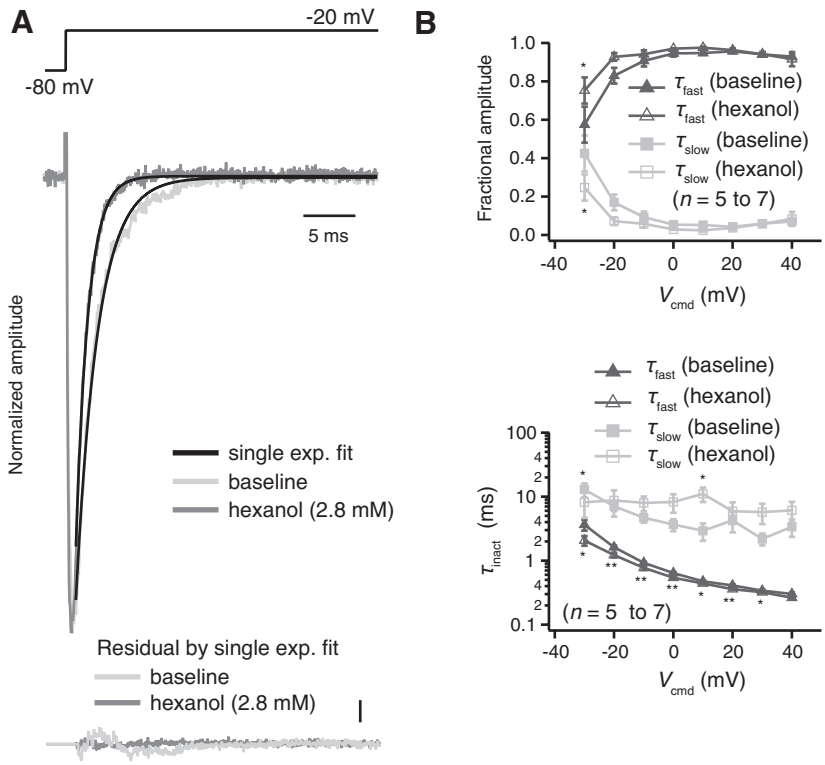

Fig. 7. Effects of hexanol on slowly inactivating component of Na^+ current. *A*: Na^+ current traces evoked by a voltage step from −80 to −20 mV in the presence and absence of 2.8 mM hexanol. The amplitudes of both currents were normalized and fit by a single-exponential function to elucidate their decaying kinetics. Scale bar in residual current traces (bottom) indicates 7% in normalized amplitude scale. *B*: group data showed that there was a significant reduction of the fractional amplitude of the slow component at −30 mV in the presence of the drug (*top*). The enhancement of fast inactivation and decrease in voltage dependence of slow component were caused by hexanol application (*bottom*). Paired *t*-test: $*P < 0.05$; $**P < 0.01$.

pyramidal neurons in slices. After neurons were isolated pharmacologically from the network (see MATERIALS AND METHODS), we first measured R_N by injecting a family of current steps (700-ms duration, from −50 to +20 pA by 10-pA increments) (Fig. 8*A*). R_N was measured by fitting a line to the steady-state voltage responses from a series of 700-ms current injections for baseline and after bath application of hexanol (1.4 mM). Possible effects on the population of ionic currents active at rest were investigated by injection of DC current to change the resting potentials, and normalized R_N vs. membrane potential is plotted in Fig. 8*B*.

We examined the effects of hexanol on the voltage threshold of an action potential evoked with current injections (120–150 pA) of 700-ms duration. Current was injected to the neuron both in the absence and presence of hexanol, and the voltage thresholds (membrane voltage of $dV/dt = 20$ mV/ms) for both conditions were compared. The amplitude of injected current was adjusted to evoke the first spike at the same latency for both conditions. There was a significant increase in voltage threshold of the first spike (−43.27 ± 1.54 vs. −38.68 ± 2.18 mV; $n = 5$; $P = 0.016$; Table 2), which was reversible on washout of hexanol (Fig. 8*C1*). In the phase plane plot of the same voltage traces, the difference in voltage threshold for both baseline and hexanol conditions can be identified (Fig. 8*C2*). There was, however, no significant change in other spike parameters such as peak dV/dt, spike amplitude, and spike half-width ($P > 0.05$; Table 2).

We also looked at the effect of hexanol on other physiological parameters: resting membrane potential, neuronal firing rate with given current injection, first spike latency, and temporal summation. In the presence of 1.4 mM hexanol, there was a hyperpolarization of the resting membrane potential of the neuron by ~2–3 mV soon after hexanol was washed in to the bath. In a separate series of experiments ($n = 5$), we investigated whether TTX and TTX with hexanol caused a similar hyperpolarization of the resting potential. TTX application caused an average hyperpolarization of 0.77 ± 0.35 mV, and TTX + hexanol caused an additional 1.37 ± 0.56 mV hyperpolarization. The voltage drop was compensated with 20–30 pA of current injection to maintain the same membrane potential as that of the baseline. With the same amplitude of sustained current injection for baseline and hexanol conditions, there was also a significant delay in the latency to the first spike from 171.4 ± 22.6 ms to 392.1 ± 71.3 ms ($n = 5$; $P = 0.016$), which was reversible by washout (Fig. 8*D*). A series of 700-ms-duration currents were injected from 30 to 180 pA by 30-pA steps, and a plot of the number of spikes vs. amplitude of current injection (F-I plot) showed a significant reversible rightward shift in the presence of hexanol, suggesting suppression of neuronal excitability by hexanol (Fig. 8*E*). Finally, the number of spikes generated by the same amplitude of α-EPSP current injections (to measure suprathreshold temporal summation) in both conditions was decreased in the presence of hexanol (2.9 ± 0.1 vs. 1.1 ± 0.4 spikes; $n = 5$; $P = 0.0077$) (Fig. 8, *F* and *G*).

DISCUSSION

Properties of I_{NaT}. The biophysical properties of I_{NaT} reported in this study are largely consistent with those reported previously for hippocampal CA1 neurons (Kuo and Bean 1994; Magee and Johnston 1995; Martina and Jonas 1997; Sah et al. 1988; Yau et al. 2010). The half-activation voltage of −21 mV was placed in the range reported from −31 mV (Sah et al. 1988) to −12.5 mV (Yau et al. 2010). The midpoint voltage of steady-state inactivation (−56.3 mV) was also within the range of previous studies (−89.5 to −55.4 mV). Different experimental conditions such as dissociated versus in vitro prepara-

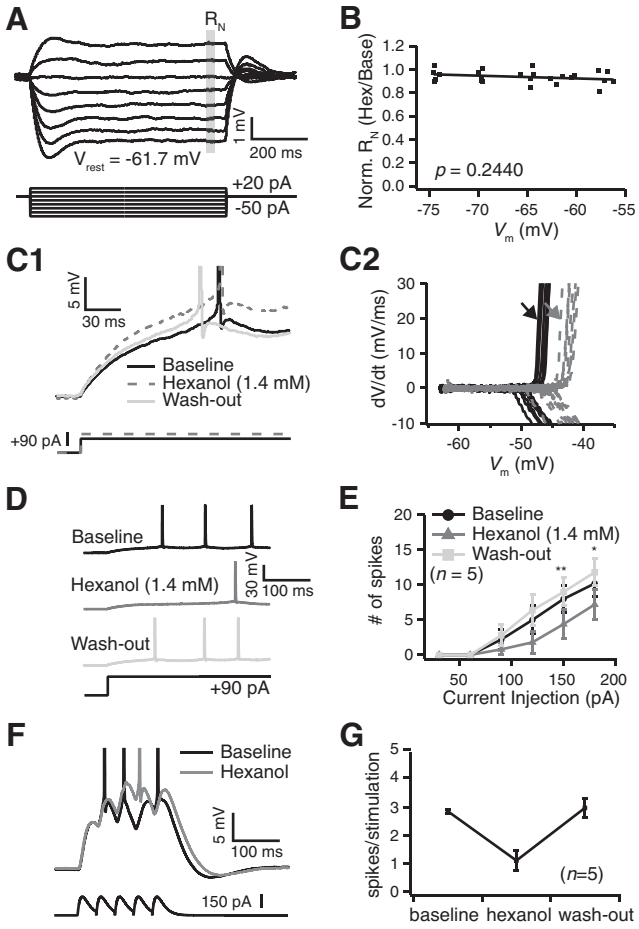

Fig. 8. Effects of hexanol on neuronal excitability. *A*: example responses to current injections of −50 pA to +20 pA by 10-pA increments. *B*: normalized input resistance ($R_{N,hexanol}/R_{N,baseline}$; $n = 5$) was measured at different holding potentials from −58 to −75 mV and showed no significant voltage dependence ($P > 0.05$; linear regression test). *C1*: 1st spike generated by a 700-ms current injection showed a significant increase in voltage threshold in the presence of hexanol, which was reversible in washout. *C2*: action potential threshold for both control and hexanol conditions. *D*: 1st spike generated by the sustained current input indicated a significant delay caused by hexanol in a reversible manner. *E*: hexanol shifted the frequency vs. current injection (F-I) curve to the right ($P < 0.01$ at 150 pA and $P < 0.05$ at 180 pA; $n = 5$; paired *t*-test). *F* and *G*: spikes generated by 5 α-EPSP injections at 25 Hz. Hexanol caused an increase in voltage threshold and a decrease in the number of spikes generated.

tion, animal species/age, recording techniques, and salt composition in external/internal solutions may contribute to this range of variation. On the other hand, our values for the kinetics of Na^+ channel gating (Figs. 3 and 4) were faster than the low end of the range in previous studies, and this likely results from the higher recording temperature used in our experiments (near physiological vs. room temperature) (Q_{10} = 2.8; Hille 2001).

The timescale of Na^+ current inactivation has a wide range that is constituted by several components of time constants ranging from few milliseconds up to several minutes (Ulbricht 2005). An intermediate slowly inactivating component of Na^+ current similar to ours was previously observed in various neuronal preparations (Jackson et al. 2004; Kononenko et al. 2004; Magistretti and Alonso 2002; Martina and Jonas 1997; Pennartz et al. 1997). For instance, a previous single Na^+ channel study reported an intermediate duration (~28 ms) of burst opening of Na^+ channel in a cortical neuron in a voltage range between −40 and 0 mV, which constitutes one of three burst opening kinetic components underlying I_{NaP} (Magistretti and Alonso 2002). I_{NaS} in the present study may reflect a similar relatively short open time of burst activity of Na^+ channel in hippocampal neurons at macroscopic current level. However, voltage independence of the medium-duration burst opening contrasted with the voltage dependence of the slow component recorded in our preparation (Fig. 4, *B* and *F*). In addition, Martina and Jonas previously reported two exponential components of Na^+ current decay kinetics in one-third of their nucleated-patch recordings in younger animals (Martina and Jonas 1997), which is similar to our results.

The decay kinetics and onset of inactivation that we observe were best fit with the sum of two exponentials where $\tau_{inact,slow}$ ranged from 4 to 125 ms in most of our nucleated patches, and this observation suggests that an additional slower (4–10 times slower) inactivating process is present during the onset of Na^+ channel inactivation. Its larger fractional amplitude around −40 to −30 mV also indicates its prominent role in that voltage range. The double-exponential components in recovery from inactivation (Fig. 4*E*), similarly reported in other studies (Martina and Jonas 1997; Yau et al. 2010), further support the presence of a second inactivation process. The second component in the deactivation kinetics at −40 mV in Fig. 3*E*, however, indicates a mixture of deactivation and inactivation of Na^+ channel at this voltage (Engel and Jonas 2005; Oxford 1981). The relative weights of the slow component (I_{NaS}) of inactivation during commands to −20 and −10 mV were different between measurements of the current decay phase (Fig. 4*B*) and that measured with a variable-duration prepulse protocol (Fig. 4*C*). In earlier experiments on squid axons (Gillespie and Meves 1980), the peak Na^+ current was increased by a sufficiently strong conditioning pulse in double pulse that had no gap between two pulses. Considering the lower activation voltage of I_{NaS} than I_{NaT} (Fig. 5*C*), the conditioning pulse at −20 and −10 mV might be strong enough to cause this effect on I_{NaS} but not on I_{NaT}. This change in peak I_{NaS} would contribute to this discrepancy.

Comparison of whole cell and nucleated-patch measurements of I_{NaP}. In whole cell somatic voltage-clamp recordings of hippocampal CA1 pyramidal neurons (Fig. 1*A*), we measured 427 pA of peak I_{NaP} amplitude (426.6 ± 62.9 MΩ; n = 30) with 254 pF whole cell capacitance (254.0 ± 10.0 pF; n = 30), using a slow (10 mV/s) ramp voltage command. The calculated I_{NaP} density current was 1.93 pA/pF (1.93 ± 0.10 pF, n = 30), which was similar to a previous report of 1.9 pA/pF peak amplitude of I_{NaP} in whole cell voltage-clamp recordings of neocortical neurons from acute slices at near-physiological temperature (Astman et al. 2006). The slow inactivation of the I_{NaP} was consistent with that seen on the 2- to 6-s timescale in other studies (Fleidervish and Gutnick 1996; Magistretti and Alonso 1999; Wu et al. 2005). If I_{NaP} were distributed evenly on the membrane, we could expect ~6.8 pA of I_{NaP} in the corresponding nucleated patch that has an average nucleated patch size of 3.5 ± 0.04 pF (n = 141). However, the Na^+ currents evoked by the same slow ramp voltage command in the peri-somatic nucleated patches did not confirm the existence of that amount of I_{NaP} (Fig. 2*B1*). Our whole cell voltage-clamp recording on the dendrotomized

Table 2. *Change in physiological parameters in the presence of hexanol*

	Baseline	Hexanol	*P* Value
Input resistance, MΩ	67.6 ± 3.4	65.4 ± 3.3	0.29
Spike threshold, mV	−43.27 ± 1.54	−38.68 ± 2.18	0.0033†
Spike peak d*V*/d*t*, mV/ms	259.8 ± 19.5	233.9 ± 14.4	0.19
Spike width, ms	1.40 ± 0.09	1.37 ± 0.08	0.34
Spike amplitude, mV	100.4 ± 2.5	98.9 ± 1.5	0.44
No. of spikes by a 700-ms step current injection of 150 pA	8.0 ± 1.9	4.4 ± 2.1	0.0061†
No. of spikes by 5 α-EPSP injections at 25 Hz	2.9 ± 0.2	1.1 ± 0.4	0.0077†
1st spike latency, ms	171.4 ± 22.6	392.1 ± 71.3	0.016*

Values are means ± SE ($n = 5$). Spike threshold was defined as a membrane voltage where dV/dt = 20 mV/ms. Spike amplitude was calculated by $V_{peak} - V_{rest}$. Paired *t*-test: *$P < 0.05$; †$P < 0.01$.

neurons suggested rather that there could exist a significant amount of I_{NaP} along the apical dendrite as well as basal dendrite and axonal area.

The steady-state inactivation of Na^+ channels in dissociated hippocampal CA1 neurons has been shown to be nearly complete, generating little steady-state current (<0.5%) considered as I_{NaP} (Kuo and Bean 1994; Taddese and Bean 2002). In experiments in which we measured I_{NaT}, the average peak I_{NaT} amplitude was 175 pA (174.6 ± 7.8; $n = 110$). If we use 0.5% proportion of I_{NaP} to I_{NaT} (Kuo and Bean 1994), the peak ramp current would be <1 pA, which might be difficult to resolve (Fig. 2*B1*).

Measurement and properties of I_{NaS}. The lack of a persistent sodium current in the nucleated patches, however, led us to try other ramp velocities, and we found a component of the macroscopic Na^+ current in response to 400 mV/s ramp commands with a peak amplitude around 7 pA (Fig. 2*B1*, *bottom*) that inactivated faster than has been described for I_{NaP} (Fleidervish and Gutnick 1996; Wu et al. 2005). The slow component of the macroscopic Na^+ current activated at more negative potentials and was kinetically and pharmacologically distinct from the fast inactivating Na^+ current, I_{NaT}. We have utilized the previous notation (Kononenko et al. 2004), I_{NaS}, to indicate its slower kinetics.

We pursued I_{NaS} measured from nucleated patches. A simple and efficient demonstration of acceptable voltage control in the nucleated patches was apparent in the currents measured in response to the ramp voltage commands of very fast velocities ranging from 800 to 8,000 mV/s (Fig. 2*E*). Those ramp voltage commands generated no unclamped Na^+ current that would be inevitable with whole cell voltage-clamp recording. We chose a velocity of 400 mV/s for inactivating I_{NaT} and allowing I_{NaS} to be measured because that gave us the largest I_{NaS} current and generated a reasonable match between the initial phase of increasing currents evoked by ramp and step protocols (Fig. 5*A*). Therefore, our ramp voltage protocol could be used to study I_{NaS} with a approach similar to that previously utilized in a Ca^{2+} current study (Corey et al. 1984). The average peak amplitude of I_{NaS} evoked by voltage ramps was 5.06 ± 0.23 pA ($n = 141$) and the current density was 1.44 ± 0.06 pA/pF, assuming 1 $\mu F/cm^2$ specific membrane capacitance. I_{NaS} showed 16.7 mV more negative $V_{1/2}$ of activation and 41.3% smaller slope factor compared with those of I_{NaT}, and its peak amplitude was linearly proportional to that of I_{NaT}.

A component of I_{Na} similar to what we call I_{NaS} was found in measurements from SCN neurons with small size, short and few processes, and high R_N (>1 GΩ, comparable to that of the nucleated patches, ~3 GΩ) (Jackson et al. 2004; Kononenko et al. 2004; Pennartz et al. 1997). Whole cell voltage clamp of intact neurons with insufficient voltage control complicates the situation because of unclamped Na^+ current elicited by the ramp voltage commands.

A component of Na^+ current with a more negative $V_{1/2}$ of activation of −62 mV in response to very slow ramps (10 mV/s) has been described in Purkinje and CA1 neurons that is able to boost synaptic events (Carter et al. 2012). These measurements were made in acutely isolated neurons with truncated processes that increased the quality of space clamp. The authors suggest that a single population of Na^+ channels with different gating modes could account for all recorded current, although they saw less slow inactivation than shown in our data and by others (Fleidervish and Gutnick 1996; Magistretti and Alonso 1999; Wu et al. 2005). The slow component of Na^+ current we described here could arise from a different population of Na^+ channels, since we recorded only from somatic nucleated patches that would not include channels in the axon initial segment or proximal dendrites, or a subset of channels that have undergone molecular change. For example, coexistence of splice variants of Na^+ channel with different kinetics, functional modifications of the channel by β-subunit, or existence of different inactivation states of the same channel could generate this component of Na^+ current (Chatelier et al. 2008; Isom et al. 1992; Payandeh et al. 2012). Although the mechanism of I_{NaS} is not clear, a hint could be obtained from a link between the closed-state inactivation present (Fig. 4*C*) and ramp current. The ramp voltage command, as an efficient method to induce closed-state inactivation, elicits a ramp current that is a mixture of I_{NaT}, I_{NaS}, and I_{NaP}. The relative contribution of each component to the total ramp current is, therefore, dependent on the ramp voltage command velocity that determines the degree of the closed-state inactivation. Others have seen a positive correlation between the magnitude of the ramp current and the degree to which the channel undergoes slow closed-state inactivation (Cummins et al. 1998). The ratio of Na^+ channels in a conformation for closed-state inactivation to those not in this state would be reflected in the amplitude of I_{NaS}, which we found to be maximized with a ramp velocity of 400 mV/s. Closed-state inactivation of Na^+ channel can occur sufficiently with movements of voltage sensor in only domains 3 and 4 (Armstrong 2006; Bähring and Covarrubias 2011). The modification of a Na^+ channel required to generate I_{NaS} might hamper the concerted conformational change of the channel resulting from the outward movement of those sensors on depolarization of

membrane potential. Then the systematic introduction of mutations onto those voltage sensors and pore domain in a way similar to the previous studies of other Na^+ channel modulators (Ragsdale et al. 1994; Sheets and Hanck 2007) could shed more light on the molecular mechanism of I_{NaS} and differential blocking of hexanol on I_{NaT} and I_{NaS}. The relative insensitivity of ranolazine to I_{NaS} in our data further suggested that the target region might reside on the nonhomologous sequences of the brain and cardiac Na^+ channels.

Physiological significance of I_{NaS}. Hexanol, riluzole, and ranolazine were used to investigate the pharmacology of I_{NaS}. The *n*-alcohols are well-known I_{NaT} blockers (Horishita and Harris 2008; Shiraishi and Harris 2004), but their effect on I_{NaS} is not known. In our results, the differential blocking of the drug on I_{NaT} and I_{NaS} (Fig. 6) and the enhanced rate of decay of Na^+ current (Fig. 7) suggested that hexanol blocks the open channel with slow binding kinetics.

To investigate the possible physiological role of this I_{NaS}, hexanol was used as a partial I_{NaS} blocker. When applied to a neuron in an intact hippocampal slice, hexanol caused a significant increase in action potential threshold (4.6 mV). Since more than a third of Na^+ channels in hippocampal neuron are redundant for single action potential initiation (Madeja 2000), 50% blocking of I_{NaS} by hexanol could explain the increased spike threshold better than differentially blocking I_{NaT} (25%). This interpretation can be further supported by three other observations: a lower voltage activation of I_{NaS}, no change in voltage dependence of I_{NaT} activation by hexanol, and no change in other active properties (Table 2). The change in other physiological parameters such as a significant delay in the first spike generated by a 700-ms current injection and reduction in the number of spikes generated in response to sustained current injections or α-EPSP injections also suggested reduced neuronal excitability of hippocampal neurons in the presence of hexanol. Although hexanol may affect other intrinsic properties, the decrease in neuronal excitability remains consistent with the reduction of I_{NaS}.

Contribution of persistent Na^+ current to neuronal excitability has been actively explored and, as an intrinsic ionic mechanism, the link between its alteration and human disease such as inherited epilepsy and pain syndromes has received intensive attention (Bean 2007; Crill 1996; Cummins et al. 2007; George 2005). However, the transient Na^+ current as well as persistent current was recently shown to activate in the subthreshold voltage range during fast depolarization and augment synaptic integration (Carter et al. 2012). The slowly inactivating component of Na^+ current in this study, which is prominent in that voltage range, might underlie at least part of such a subthreshold Na^+ current. This slowly inactivating component of the macroscopic Na^+ current may play an important role in determining neuronal excitability since it plays a role near the threshold for spike generation in the intact neuron. Understanding its properties may provide valuable insight into how an intrinsic mechanism can regulate neuronal activity and could be a new therapeutic target for channelopathies underlain by the Na^+ channel.

GRANTS

This work was supported by National Institute of Mental Health Grant MH-048432 (to D. Johnston).

DISCLOSURES

No conflicts of interest, financial or otherwise, are declared by the author(s).

AUTHOR CONTRIBUTIONS

Author contributions: Y.Y.P., D.J., and R.G. conception and design of research; Y.Y.P. performed experiments; Y.Y.P. analyzed data; Y.Y.P., D.J., and R.G. interpreted results of experiments; Y.Y.P. prepared figures; Y.Y.P. and R.G. drafted manuscript; Y.Y.P., D.J., and R.G. edited and revised manuscript; Y.Y.P., D.J., and R.G. approved final version of manuscript.

REFERENCES

Alifimoff JK, Firestone LL, Miller KW. Anaesthetic potencies of primary alkanols: implications for the molecular dimensions of the anaesthetic site. *Br J Pharmacol* 96: 9–16, 1989.

Armstrong CM. Na channel inactivation from open and closed states. *Proc Natl Acad Sci USA* 103: 17991–17996, 2006.

Astman N, Gutnick MJ, Fleidervish IA. Persistent sodium current in layer 5 neocortical neurons is primarily generated in the proximal axon. *J Neurosci* 26: 3465–3473, 2006.

Bähring R, Covarrubias M. Mechanisms of closed-state inactivation in voltage-gated ion channels. *J Physiol* 589: 461–479, 2011.

Bean BP. The action potential in mammalian central neurons. *Nat Rev Neurosci* 8: 451–465, 2007.

Benoit E, Corbier A, Dubois JM. Evidence for two transient sodium currents in the frog node of Ranvier. *J Physiol* 361: 339–360, 1985.

Benoit E, Escande D. Riluzole specifically blocks inactivated Na channels in myelinated nerve fibre. *Pflügers Arch* 419: 603–609, 1991.

Carter BC, Giessel AJ, Sabatini BL, Bean BP. Transient sodium current at subthreshold voltages: activation by EPSP waveforms. *Neuron* 75: 1081–1093, 2012.

Chatelier A, Dahllund L, Eriksson A, Krupp J, Chahine M. Biophysical properties of human $Na_v1.7$ splice variants and their regulation by protein kinase A. *J Neurophysiol* 99: 2241–2250, 2008.

Chiu SY. Inactivation of sodium channels: second order kinetics in myelinated nerve. *J Physiol* 273: 573–596, 1977.

Corey DP, Dubinsky JM, Schwartz EA. The calcium current in inner segments of rods from the salamander (*Ambystoma tigrinum*) retina. *J Physiol* 354: 557–575, 1984.

Crill WE. Persistent sodium current in mammalian central neurons. *Annu Rev Physiol* 58: 349–362, 1996.

Cummins TR, Howe JR, Waxman SG. Slow closed-state inactivation: a novel mechanism underlying ramp currents in cells expressing the hNE/PN1 sodium channel. *J Neurosci* 18: 9607–9619, 1998.

Cummins TR, Sheets PL, Waxman SG. The roles of sodium channels in nociception: implications for mechanisms of pain. *Pain* 131: 243–257, 2007.

Cummins TR, Xia Y, Haddad GG. Functional properties of rat and human neocortical voltage-sensitive sodium currents. *J Neurophysiol* 71: 1052–1064, 1994.

Engel D, Jonas P. Presynaptic action potential amplification by voltage-gated Na^+ channels in hippocampal mossy fiber boutons. *Neuron* 45: 405–417, 2005.

Fleidervish IA, Gutnick MJ. Kinetics of slow inactivation of persistent sodium current in layer V neurons of mouse neocortical slices. *J Neurophysiol* 76: 2125–2130, 1996.

George AL. Inherited disorders of voltage-gated sodium channels. *J Clin Invest* 115: 1990–1999, 2005.

Gillespie JI, Meves H. The time course of sodium inactivation in squid giant axons. *J Physiol* 299: 289–307, 1980.

Gilly WF, Armstrong CM. Threshold channels—a novel type of sodium channel in squid giant axon. *Nature* 309: 448–450, 1984.

Hille B. *Ion Channels of Excitable Membranes*. Sunderland, MA: Sinauer, 2001.

Horishita T, Harris RA. *n*-Alcohols inhibit voltage-gated Na^+ channels expressed in *Xenopus* oocytes. *J Pharmacol Exp Ther* 326: 270–277, 2008.

Huguenard JR, Hamill OP, Prince DA. Developmental changes in Na^+ conductances in rat neocortical neurons: appearance of a slowly inactivating component. *J Neurophysiol* 59: 778–795, 1988.

Isom LL, De Jongh KS, Patton DE, Reber BF, Offord J, Charbonneau H, Walsh K, Goldin AL, Catterall WA. Primary structure and functional expression of the beta 1 subunit of the rat brain sodium channel. *Science* 256: 839–842, 1992.

Jackson AC, Yao GL, Bean BP. Mechanism of spontaneous firing in dorsomedial suprachiasmatic nucleus neurons. *J Neurosci* 24: 7985–7998, 2004.

Kang H, Schuman EM. A requirement for local protein synthesis in neurotrophin-induced hippocampal synaptic plasticity. *Science* 273: 1402–1406, 1996.

Kononenko NI, Shao LR, Dudek FE. Riluzole-sensitive slowly inactivating sodium current in rat suprachiasmatic nucleus neurons. *J Neurophysiol* 91: 710–718, 2004.

Kuo CC, Bean BP. Na^+ channels must deactivate to recover from inactivation. *Neuron* 12: 819–829, 1994.

Madeja M. Do neurons have a reserve of sodium channels for the generation of action potentials? A study on acutely isolated CA1 neurons from the guinea-pig hippocampus. *Eur J Neurosci* 12: 1–7, 2000.

Magee JC, Johnston D. Characterization of single voltage-gated Na^+ and Ca^{2+} channels in apical dendrites of rat CA1 pyramidal neurons. *J Physiol* 487: 67–90, 1995.

Magistretti J, Alonso A. Biophysical properties and slow voltage-dependent inactivation of a sustained sodium current in entorhinal cortex layer-II principal neurons: a whole-cell and single-channel study. *J Gen Physiol* 114: 491–509, 1999.

Magistretti J, Alonso A. Fine gating properties of channels responsible for persistent sodium current generation in entorhinal cortex neurons. *J Gen Physiol* 120: 855–873, 2002.

Martina M, Jonas P. Functional differences in Na^+ channel gating between fast-spiking interneurones and principal neurones of rat hippocampus. *J Physiol* 505: 593–603, 1997.

Oxford GS. Some kinetic and steady-state properties of sodium channels after removal of inactivation. *J Gen Physiol* 77: 1–22, 1981.

Payandeh J, Gamal El-Din TM, Scheuer T, Zheng N, Catterall WA. Crystal structure of a voltage-gated sodium channel in two potentially inactivated states. *Nature* 486: 135–139, 2012.

Pennartz CM, Bierlaagh MA, Geurtsen AM. Cellular mechanisms underlying spontaneous firing in rat suprachiasmatic nucleus: involvement of a slowly inactivating component of sodium current. *J Neurophysiol* 78: 1811–1825, 1997.

Provencher SW. An eigenfunction expansion method for the analysis of exponential decay curves. *J Chem Phys* 64: 2772–2777, 1976.

Ragsdale DS, McPhee JC, Scheuer T, Catterall WA. Molecular determinants of state-dependent block of Na^+ channels by local anesthetics. *Science* 265: 1724–1728, 1994.

Rajamani S, El-Bizri N, Shryock JC, Makielski JC, Belardinelli L. Use-dependent block of cardiac late Na^+ current by ranolazine. *Heart Rhythm* 6: 1625–1631, 2009.

Raman IM, Bean BP. Resurgent sodium current and action potential formation in dissociated cerebellar Purkinje neurons. *J Neurosci* 17: 4517–4526, 1997.

Sah P, Gibb AJ, Gage PW. The sodium current underlying action potentials in guinea pig hippocampal CA1 neurons. *J Gen Physiol* 91: 373–398, 1988.

Sheets MF, Hanck DA. Outward stabilization of the S4 segments in domains III and IV enhances lidocaine block of sodium channels. *J Physiol* 582: 317–334, 2007.

Shiraishi M, Harris RA. Effects of alcohols and anesthetics on recombinant voltage-gated Na^+ channels. *J Pharmacol Exp Ther* 309: 987–994, 2004.

Spruston N, Jaffe DB, Williams SH, Johnston D. Voltage- and space-clamp errors associated with the measurement of electrotonically remote synaptic events. *J Neurophysiol* 70: 781–802, 1993.

Taddese A, Bean BP. Subthreshold sodium current from rapidly inactivating sodium channels drives spontaneous firing of tuberomammillary neurons. *Neuron* 33: 587–600, 2002.

Ulbricht W. Sodium channel inactivation: molecular determinants and modulation. *Physiol Rev* 85: 1271–1301, 2005.

Williams SR, Mitchell SJ. Direct measurement of somatic voltage clamp errors in central neurons. *Nat Neurosci* 11: 790–798, 2008.

Wu N, Enomoto A, Tanaka S, Hsiao CF, Nykamp DQ, Izhikevich E, Chandler SH. Persistent sodium currents in mesencephalic V neurons participate in burst generation and control of membrane excitability. *J Neurophysiol* 93: 2710–2722, 2005.

Yau HJ, Baranauskas G, Martina M. Flufenamic acid decreases neuronal excitability through modulation of voltage-gated sodium channel gating. *J Physiol* 588: 3869–3882, 2010.